A numerical analysis of CPT-based tip resistance prediction during pile installation in clays

Shujin Zhou[1#], *Wangcheng* Zhang[1], and *Ashraf* Osman[1]

[1]*Department of Engineering, Durham University, South Road, Durham, DH1 3LE, UK.*
[#]*Corresponding author: shujin.zhou@durham.ac.uk*

ABSTRACT

Accurately predicting the installation resistance of offshore piles is important for their design and application. The cone penetration test (CPT) is the most widely used in situ sounding tests for pile drivability analysis and capacity prediction. While there are established empirical correlation methods to connect CPT data with pile installation resistance, the underlying mechanisms behind these correlations have yet to be fully understood. This study performs a numerical analysis to reveal such mechanisms and improve the correlations. The pile installation and cone penetration processes are modelled using a large-deformation finite-element method. For all analyses, a smooth cone and a smooth pile are simulated to quantify the relationship of tip resistance between the pile and CPT. The mechanisms of the two analogous penetration processes are visualized and compared through numerical modelling. As the cone advances, it pushes the soil at the cone tip into the far field. During the pile penetration process, soil heaving can be observed with the soil surface inside the pile moving above the mudline. The soil failure is localized at a small zone around the pile tip. The penetration resistances of pile are correlated to CPT data with the aid of numerical modelling and compared to existing CPT-based design guidelines. A discussion on the pile tip resistance correlated with cone tip resistance is included, and the value of the empirical coefficient for tip resistance k_p is obtained.

Keywords: Pile installation; cone penetration test; clay; large-deformation finite-element method.

1. Introduction

Offshore pile foundations have been extensively employed to support offshore renewables and traditional oil/gas facilities, such as manifolds, terminations, tension legs, and spar platforms (Chen and Randolph 2007, Doherty and Gavin 2011). The application versatility is being broadened due to their ease of installation and cost effectiveness.

To determine the resistance profile of pile penetration in soils, one proper solution is employing mechanism-based methods (Houlsby and Byrne 2005a, 2005b), which were derived from bearing capacity theories with proper assumptions and simplifications. However, the shear strength of soils considered in the mechanism-based approaches is often obtained from laboratory geotechnical elementary tests and can be rather different from the one in situ. To improve the uncertainties of soil samples from laboratory tests, the pile penetration resistance is alternatively estimated with in situ cone penetration test (CPT) results, as it provides nearly continuous record of the resistance with depth. Both DNV (Det Norske Veritas) (DNV 2017) and NGI (Norwegian Geotechnical Institute) (Clausen et al. 2005) guidelines recommend CPT-based methods to predict the penetration resistance assisted with relevant laboratory testing results.

Mechanism-based prediction method of pile penetration resistance using the bearing capacity theory has been proposed by Houlsby and Byrne (2005a) for clay and Houlsby and Byrne (2005b) for sand. For clay, the total resistance to penetration V can be expressed as

$$V = \alpha s_{\mathrm{u,av}} A_{\mathrm{s}} + \left(N_{\mathrm{c}} s_{\mathrm{u,t}} + \gamma' d\right) A_{\mathrm{t}} \quad (1)$$

where α is the adhesion factor; $s_{\mathrm{u,av}}$ is the average shear strength of soil over the penetration depth, d; $s_{\mathrm{u,t}}$ is the shear strength of soil at the pile tip level; N_{c} is the bearing capacity factor (typically a value of about 9 is adopted with reference to a deep penetration mechanism (API 2000, Houlsby and Byrne 2005a)); γ' is the effective unit weight; A_{s} and A_{t} are the pile wall area and tip area, respectively.

Since a cone penetrometer and a pile are similar in geometry, the CPT data is often directly related to the pile installation resistance (Almeida et al. 1996, Jardine et al. 2005, Lehane et al. 2000). According to Jardine et al. (2005), pile installation resistance can be calculated, with the wall friction being in the effective stress framework, by:

$$V = k_{\mathrm{p}} q_{\mathrm{c}} A_{\mathrm{t}} + \pi D \int \tau_{\mathrm{f}}\, dz \quad (2)$$

$$\tau_{\mathrm{f}} = \sigma_{\mathrm{rf}}^{'} \tan \delta_{\mathrm{f}} \quad (3)$$

$$\sigma_{\mathrm{rf}}^{'} = 0.8 \sigma_{\mathrm{rc}}^{'} \quad (4)$$

$$\sigma_{\mathrm{rc}}^{'} = K_{\mathrm{c}} \sigma_{\mathrm{v0}}^{'} \quad (5)$$

$$K_{\mathrm{c}} = [2.2 + 0.016\mathrm{OCR} - 0.87 \log_{10}(S_{\mathrm{t}})]\mathrm{OCR}^{0.42} F_{\mathrm{L}} \quad (6)$$

where q_{c} is the CPT tip resistance; k_{p} is the empirical coefficient relating q_{c} to end resistance; τ_{f} is the peak shear stress on pile shaft; σ'_{rf} is the radial effective stress at failure; σ'_{rc} is the radial effective stress after

equalization; δ_f is the clay-pile interface friction angle; K_c is the earth pressure coefficient after full setup; σ'_{v0} is the in situ vertical stress; OCR is the over-consolidation ratio; S_t is the soil sensitivity; $F_L = (h/R)^{-0.2} \geq 8.0$; h is the distance from the pile tip; and R is the pile radius. Lehane et al. (2022) also used a database of displacement piles and proposed an alternative CPT-based form to Eq. (3), where the wall friction is related to the CPT tip resistance and soil sensitivity.

A direct CPT-based design method was proposed by DNV (2017), where both the tip resistance and wall friction are related to the CPT tip resistance, i.e.

$$V = k_p(d)A_t q_c + A'_s \int_0^d k_f(z) q_c(z)\, dz \quad (7)$$

where $k_p(d)$ = empirical coefficient relating q_c to pile end resistance during installation, ranging from 0.4 to 0.6 for clay; $k_f(z)$ = empirical coefficient relating q_c to pile skin friction, ranging from 0.03 to 0.05 for clay; A'_s is the side area of penetrating member, per unit penetration depth.

Although CPTs are commonly used for the design and analysis of piles, quantification of the coefficients (e.g., k_p and k_f) remains a challenge since their empirical values are determined based on certain site test conditions, which could hinder the widespread use of the figures. The underlying mechanisms of both CPT and pile installation need to be understood and compared to reveal a more accurate correlation between their penetration resistances. Laboratory visualization of the soil flow mechanism is extremely difficult, if not entirely impossible. A comprehensive analysis involving numerical modelling is required to thoroughly investigate the correlation between pile resistance and CPT data, and to validate or improve the existing design methods.

2. Numerical modelling

2.1. LDFE analyses

Geotechnical applications in offshore engineering often involve significant displacement of structural elements. Simulation of offshore soil-structure interaction needs to consider nonlinearity arising from moving boundary and material flow. To tackle the excessive mesh distortion because of large deformation in traditional small strain FE method, significant efforts have been made in developing more advanced numerical tools, such as the Arbitrary Lagrangian Eulerian (ALE) method, the Material Point Method (MPM), and the coupled Eulerian-Lagrangian (CEL) method (Fan et al. 2021, Phuong et al. 2014, Zhou et al. 2021). In this study, the RITSS method (Remeshing and interpolation technique with small strain (Hu and Randolph 1998)) is developed and implemented in the commercial software ABAQUS, where the whole penetration process is divided into a series of incremental small strain analyses combined with frequent remeshing of the entire domain, followed by updating all field variables (i.e., stresses and material properties) from the old mesh to the new mesh.

2.2. Geometry and parameters

As illustrated schematically in Figure 1, the piezocone model has a cone area of 1500 mm^2 (diameter D_c = 43·7 mm) and a tip–apex angle of 60° (Boggess and Robertson 2011, Randolph and Gourvenec 2017). The pipe pile of an outer diameter D_p = 1.0 m, a length L = 10 m (i.e., L/D_p = 10), a wall thickness t = 0.02 m (i.e., D_p/t = 50) is considered in the numerical modelling. The pile and the cone are simplified as rigid bodies since their stiffness greatly exceeds that of the soil.

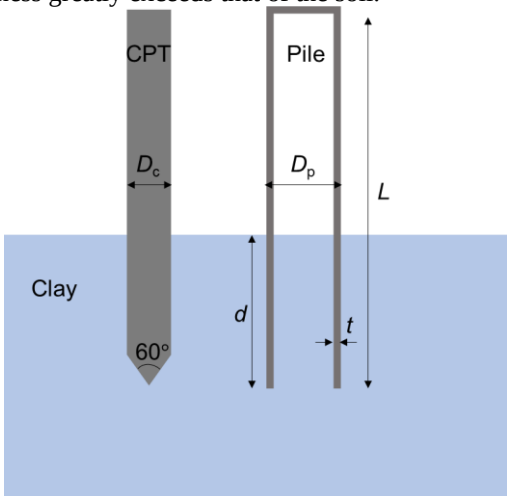

Figure 1. Schematic cone penetrometer and pile into soil ground.

The axisymmetric soil domain is chosen as 15 m in radius and 30 m in depth to ensure that the domain boundaries are well outside the soil plastic zone through the whole penetration process. Displacements are fixed in all directions at the soil base, whereas null radial movement is prescribed in the two vertical faces. Linear four-node quadrilateral elements (CAX4) with four internal Gauss points (full integration) are used in the FE analyses. Fine mesh is used around the cone/pile tip to ensure the accuracy of the numerical results, while coarse mesh is employed when the domain experiences minimal disruption due to the penetration process. Figure 2 displays the initial mesh and boundary conditions for CPT and pile, respectively.

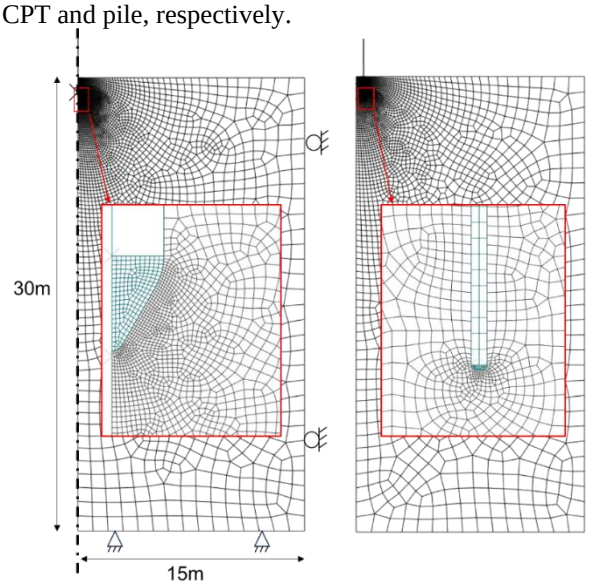

Figure 2. Initial mesh for cone and pile penetration.

The soil is modelled as a linear elastic-perfectly plastic material. Considering a relatively fast penetration rate and low permeability of clays, undrained soil condition is assumed with a Poisson's ratio of $\nu = 0.495$ and a Tresca yield criterion used in the numerical modelling. The undrained shear strength is taken as s_u = 5 kPa and the submerged soil density is $\rho' = 600$ kg/m^3. The Young's modulus is set to $E = 300s_u$ and hence the rigidity index is $I_r \approx 100$. Isotropic geostatic stress condition is generated with using $K_0 = 1$. It is noted that some parameters used in the validation analysis (Section 2.3) are different and referred to previous studies.

2.3. Model validation

The simulation of CPT process is validated against existing solutions. The analysis is conducted to explore the effect of soil rigidity index I_r, varying from 50 to 500. The results are compared with several existing solutions including those from Yu (2000), Lu et al. (2004), Liyanapathirana (2009), Zheng (2015), and Martinelli and Galavi (2022) as shown in Figure 3. It can be seen that, the bearing factors, N_{kt} (discussed in Section 3.1), derived from the present work generally agree well with the RITSS method (Lu et al. 2004), CEL technique (Zheng 2015), the MPM approach (Martinelli and Galavi 2022), and slightly larger than the results from ALE method by Liyanapathirana (2009) and cavity expansion method by Yu (2000).

Validation of the pile penetration modelling is performed against centrifuge test available in the literature (Chen and Randolph 2007). The equivalent prototype pile of outer diameter D_p = 3.6 m, length L = 14.4 m, and wall thickness t = 0.06 m was installed in kaolin clay with undrained shear strength $s_u = 1.17z$ kPa where z is the depth, soil sensitivity S_t = 2 ~ 2.8 and effective unit weight $\gamma' = 6.86$ kN/m^3. The undrained shear strength is taken as $s_u = 0.1 + 1.17z$ in the FE model where the minimal mudline strength of 0.1 kPa is set to maintain numerical stability, and the adhesion factor α = 0.35 is adopted with reference to the back-calculated analysis from Chen and Randolph (2007). Figure. 4 shows consistent profiles of penetration resistance from centrifuge data, analytical results (Houlsby and Byrne 2005a) and current LDFE analysis.

The close agreements between the LDFE results with the documented results of CPT and pile installation provide confidence in the numerical model used and ensure the accuracy of the corresponding results.

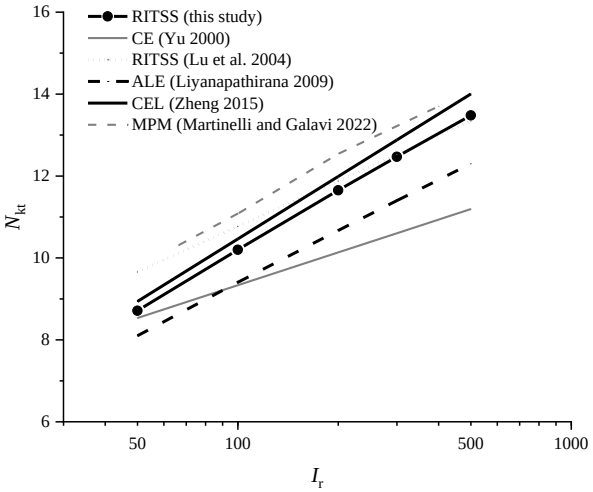

Figure 3. Comparison of cone factor N_{kt} with previous theoretical solutions. (CE: cavity expansion theory; ALE: arbitrary Lagrangian-Eulerian method; CEL: coupled Eulerian-Lagrangian method; MPM: Material Point Method)

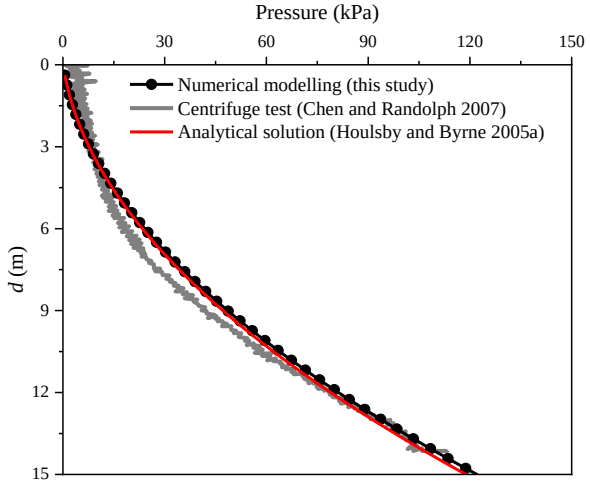

Figure 4. Comparison of penetration resistances from analytical, numerical and centrifuge test results.

3. Results and discussion

3.1. Soil flow mechanisms and resistances

Figure 5 shows the failure mechanism when the cone is penetrated to a depth of $60D_c$, where the left sub-figure shows the normalized incremental displacement vectors (Δu and Δu_c are the incremental displacement of soil and cone, respectively), and the right sub-figure presents the contour of Tresca stress ($\sigma_1 - \sigma_3$, where σ_1 and σ_3 denote the maximum and minimum principal stresses, respectively). It is noted that both CPT and pile are pre-embedded in soil at a depth of 1 m. It can be seen that for penetrating a smooth cone the soil failure is observed around the cone tip, and soils near the shaft of 1 m below the mudline (pre-embedded depth) remains undisturbed. As the cone advances, it pushes the material at the tip of the cone into the far field.

For clay deposits, the cone factor N_{kt} is used to correlate the net cone tip resistance q_{net} to the intact undrained shear strength s_u as

$$N_{kt} = \frac{q_{net}}{s_u} = \frac{q_c - \sigma_{v0}}{s_u} \quad (8)$$

where q_c is the cone tip resistance and σ_{v0} is the overburden stress. The bearing capacity factor (N_{kt}) over penetration depth (d/D_p) is plotted in Fig. 6. It is shown that the cone factor N_{kt} is stabilized at a deep penetration depth, where N_{kt} is found to be 10.2.

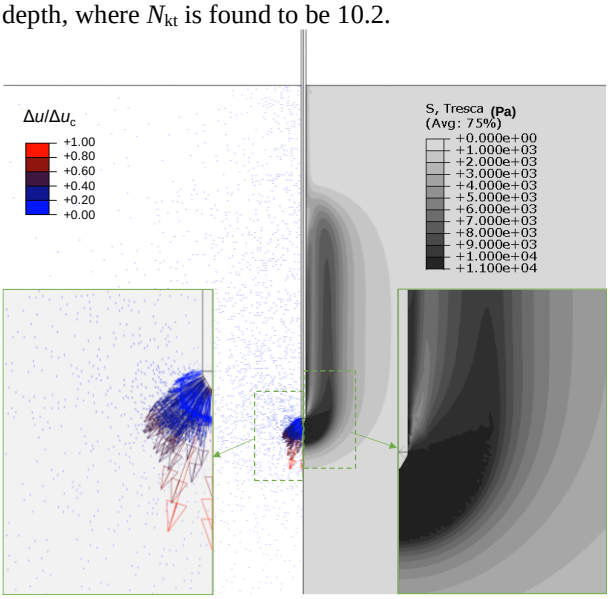

Figure 5. Soil flow mechanism for CPT penetration at a depth of $60D_c$.

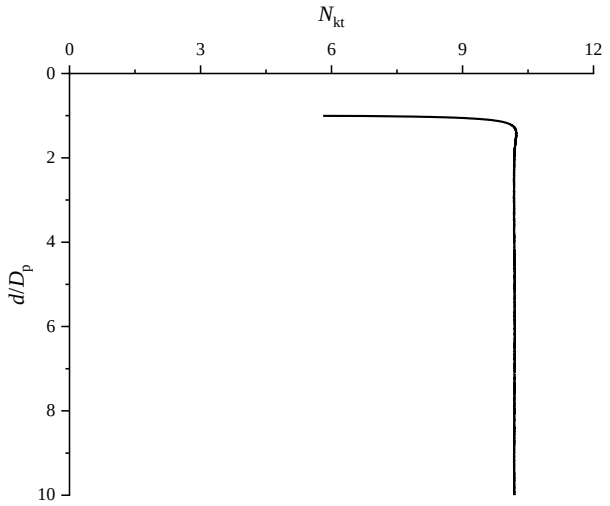

Figure 6. The bearing factor N_{kt} for a smooth cone.

The soil flow mechanism for pile penetration at a depth of $4D_p$ or $200t$ is shown in Fig. 7, where the left half shows the normalized incremental displacement vectors (Δu_p is the incremental displacement of pile), and the right half gives the contour of Tresca stress. It is shown that the soils inside the pipe pile flows upward, and significant soil heave can be observed at the surface of inner soils. As the pile penetrates, it compresses part of the soil beneath the pile (from the centerline of the problem up to the external interface of the pile), forcing the soil into the interior of the pile while pushing another part of soil into the far field, which contributes to the development of inner soil heave. This plastic failure mechanism has been previously discussed by Monforte et al. (2022). The end bearing resistances of CPT and pile are related with the localized plastic area around the tip.

Fig. 8 displays the end bearing capacity factor, N_c, against normalized penetration depth, d/D_p. For a smooth pile, N_c is approximately equal to 9 and slightly increases with the penetration depth. This value is analogous to the bearing capacity factor for a deep strip footing in clay, which is popularly adopted in the pipe pile design (Houlsby and Byrne 2005a, Westgate et al. 2009). The slightly increasing trend is due to the inner soil heave, since the extra overburden due to soil heave is not considered in σ_{v0} in Eq. 8.

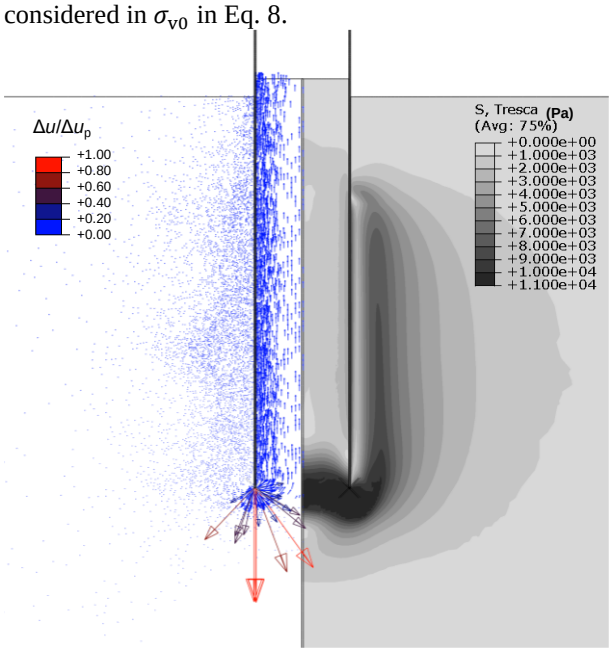

Figure 7. Soil flow mechanisms for pile penetration at a depth of $4D_p$.

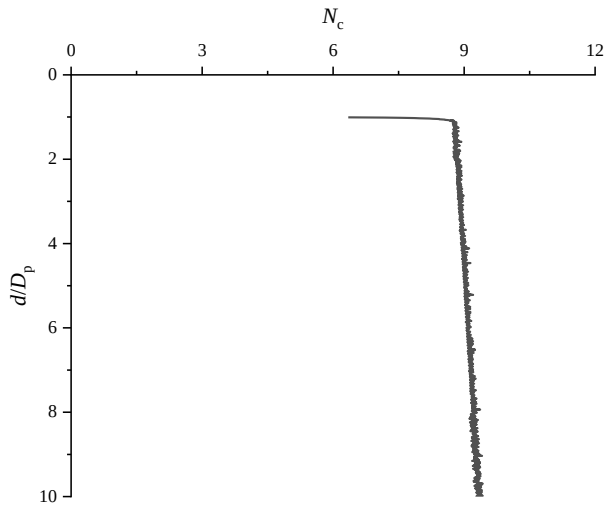

Figure 8. Bearing capacity factor, N_c, for pile penetration.

3.2. Prediction of pile tip resistance based on CPT data

The correlation of pile tip resistance, q_t, with cone tip resistance, q_c, can be obtained by two methods, i.e., the bearing capacity-based method and the direct correlation method. The sole distinction between these two methods lies in the explicit consideration of σ_{v0}. For the bearing capacity-based method,

$$q_t = N_c s_u + \sigma_{v0} \tag{9}$$

As mentioned above, the cone tip resistance q_c can be calculated according to Eq. 8. The ratio of capacity factor k'_p is calculated as follows:

$$k'_{\mathrm{p}} = \frac{N_{\mathrm{c}}}{N_{\mathrm{kt}}} \quad (10)$$

Eq. 9 can be written as:

$$q_{\mathrm{t}} = k'_{\mathrm{p}} q_{\mathrm{net}} + \sigma_{\mathrm{v0}} \quad (11)$$

For a direct CPT-based design method, pile tip resistance, q_{t}, can be calculated as

$$q_{\mathrm{t}} = k_{\mathrm{p}} q_{\mathrm{c}} \quad (12)$$

The results of k'_{p} and k_{p} are depicted in Fig. 9, from which it can be seen that k_{p} is slightly larger than k'_{p}. Overall, both k'_{p} and k_{p} lie in a range from 0.85 to 0.95. Doherty et al. (2010) reported a unique set of measurements featuring a twin-walled instrumented pile, which facilitated the differentiation between the average stress at the base of the plug and the stress on the annulus during pile installation. Their findings revealed that the end resistance developed by the open-ended piles (q_{t}) were similar to cone tip resistance (q_{c}), falling in a range of 0.8 to 1.2, aligning with the results of this study. However, the k_{p} values of this study exceed the recommendations (0.4 ~ 0.6) by DNV (2017).

It should be noted that only frictionless contact interfaces are considered in this study. Since the roughness of cone/soil and pile/soil may be different in practice, and soil plug may occur during pile installation with a large roughness, the values of k'_{p} and k_{p} could be more scattered. Also, it is acknowledged that the effect of soil stiffness on the cone tip resistance is significant, whereas its influence on the pile tip resistance remains uncertain. Further studies about pile/soil roughness and soil stiffness are needed.

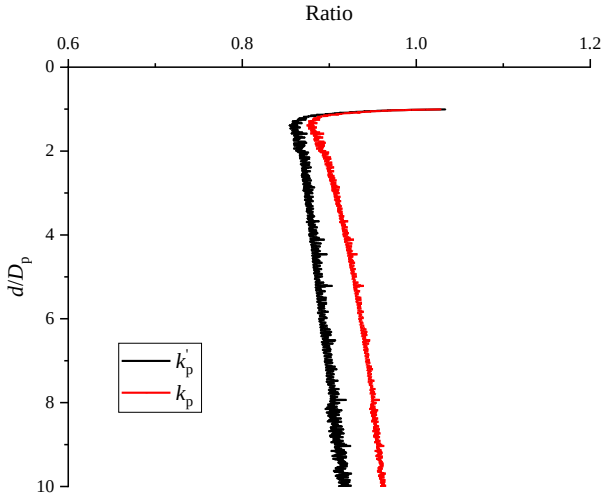

Figure 9. Distribution of k'_{p} and k_{p} values.

4. Conclusions

The behaviors of a cone penetrometer and a pipe pile penetrating through uniform clay have been studied through a large deformation finite element analysis. The results are validated against existing theoretical solutions and centrifuge test, with reasonable agreement obtained. The soil flow mechanism and penetration resistance for a smooth pile are investigated. For pile penetration, soil heaving is developed with the soil surface inside the pile moving above the mudline. The soil failure is localized at a small zone around the pile tip. The penetration resistance of the pile is correlated to cone tip resistance and a CPT-based design approach is improved based on the numerical results. A practical range of empirical coefficients k_{p} and k'_{p} are discussed in detail. It can be concluded that k'_{p} and k_{p} lie in a range from 0.85 to 0.95.

Acknowledgements

The first author is the recipient of the Durham-CSC (China Scholarship Council) Joint PhD Scholarship (CSC 202206150024).

References

Almeida, M. S. S., Danziger, F. A. B., and Lunne, T. 1996. "Use of the piezocone test to predict the axial capacity of driven and jacked piles in clay." Canadian Geotechnical Journal, 33(1), 23-41. https://doi.org/10.1139/t96-022

API (American Petroleum Institute). 2000. "Recommended practice for planning, designing and constructing fixed offshore platforms." In. Washington, DC.

Boggess, R., and Robertson, P. 2011. "CPT for soft sediments and deepwater investigations." In offshore technology conference (pp. OTC-21244). OTC. https://doi.org/10.4043/21244-MS

Chen, W., and Randolph, M. 2007. "External radial stress changes and axial capacity for suction caissons in soft clay." Géotechnique, 57(6), 499-511. https://doi.org/10.1680/geot.2007.57.6.499

Clausen, C., Aas, P., and Karlsrud, K. 2005. "Bearing capacity of driven piles in sand, the NGI approach." Proceedings of International Symposium on Frontiers in Offshore Geotechnics, Perth.

DNV, G. 2017. "Offshore soil mechanics and geotechnical engineering." Offshore Standard DNVGL-RP-C212, Edition August.

Doherty, P., and Gavin, K. 2011. "Shaft capacity of open-ended piles in clay." Journal of Geotechnical and Geoenvironmental Engineering, 137(11), 1090-1102. https://doi.org/10.1061/(ASCE)GT.1943-5606.0000528

Doherty, P., Gavin, K., and Gallagher, D. 2010. "Field investigation of base resistance of pipe piles in clay." Proceedings of the Institution of Civil Engineers-Geotechnical Engineering 163(1):13-22. https://doi.org/10.1680/geng.2010.163.1.13

Fan, S., Bienen, B. and Randolph, M. F. 2021. "Effects of monopile installation on subsequent lateral response in sand. I: Pile installation." Journal of Geotechnical and Geoenvironmental Engineering, 147(5):04021021. https://doi.org/10.1061/(ASCE)GT.1943-5606.0002467

Focht, J. A., and Vijayvergiya, V. 1972. "A new way to predict capacity of piles in clay." Offshore Technology Conference. https://doi.org/10.4043/1718-MS

Houlsby, G. T., and Byrne, B. W. 2005a. "Design procedures for installation of suction caissons in clay and other materials." Proceedings of the Institution of Civil Engineers-Geotechnical Engineering, 158(2), 75-82. https://doi.org/10.1680/geng.2005.158.2.75

Houlsby, G. T., and Byrne, B. W. 2005b. "Design procedures for installation of suction caissons in sand." Proceedings of the Institution of Civil Engineers-Geotechnical Engineering, 158(3), 135-144. https://doi.org/10.1680/geng.2005.158.3.135

Hu, Y., and Randolph, M. 1998. "A practical numerical approach for large deformation problems in soil." International Journal for Numerical and Analytical Methods in Geomechanics, 22(5), 327-350. https://doi.org/10.1002/(SICI)10969853(199805)22:5<327::AID-NAG920>3.0.CO;2-X

Jardine, R., Chow, F., Overy, R., and Standing, J. 2005. “ICP design methods for driven piles in sands and clays.” Thomas Telford Publishing.

Lehane, B., Lim, J. K., Carotenuto, P., Nadim, F., Lacasse, S., Jardine, R., and Van Dijk, B. 2017. “Characteristics of unified databases for driven piles.” Proceedings of the 8th International Conference of Offshore Site Investigation and Geotechnics OSIG, London, UK. https://doi.org/10.3723/OSIG17.162

Lehane, B. M., Chow, F., McCabe, B., and Jardine, R. 2000. “Relationships between shaft capacity of driven piles and CPT end resistance.” Proceedings of the Institution of Civil Engineers-Geotechnical Engineering, 143(2), 93-101. https://doi.org/10.1680/geng.2000.143.2.93

Lehane, B. M., Liu, Z. Q., Bittar, E. J., Nadim, F., Lacasse, S., Bozorgzadeh, N., Morgan, N. 2022. “CPT-Based Axial Capacity Design Method for Driven Piles in Clay.” Journal of Geotechnical and Geoenvironmental Engineering, 148(9). https://doi.org/10.1061/(ASCE)GT.1943-5606.0002847

Liyanapathirana, D. S. 2009. “Arbitrary Lagrangian Eulerian based finite element analysis of cone penetration in soft clay.” Computers and Geotechnics, 36(5), 851-860. https://doi.org/10.1016/j.compgeo.2009.01.006

Lu, Q., Randolph, M. F., Hu, Y., and Bugarski, I. C. 2004. “A numerical study of cone penetration in clay.” Géotechnique, 54(4), 257-267. https://doi.org/10.1680/geot.2004.54.4.257

Martinelli, M., and Galavi, V. 2022. “An explicit coupled MPM formulation to simulate penetration problems in soils using quadrilateral elements.” Computers and Geotechnics, 145, 104697. https://doi.org/10.1016/j.compgeo.2022.104697

Monforte, L., Arroyo, M., Carbonell, J. M., and Gens, A. (2022). “Large-strain analysis of undrained smooth tube sampling.” Geotechnique, 72(1), 61-77. https://doi.org/10.1680/jgeot.19.P.354

Phuong, N., Van Tol, A., Elkadi, A. and Rohe, A. 2014. “Modelling of pile installation using the material point method (MPM).” Numerical methods in Geotechnical engineering 271:271-276. https://doi.org/10.1201/b17017-50

Randolph, M., and Gourvenec, S. 2017. Offshore Geotechnical Engineering. CRC Press. https://doi.org/10.1201/9781315272474

Westgate, Z., Tapper, L., Lehane, B., and Gaudin, C. 2009. “Modelling the installation of stiffened caissons in overconsolidated clay.” International Conference on Offshore Mechanics and Arctic Engineering. https://doi.org/10.1115/OMAE2009-79125

Yu, H.-S. 2000. “Cavity expansion methods in geomechanics.” Springer Science and Business Media.

Zheng, J. 2015. “Numerical modelling of spudcan and cone penetration in multi-layer soils.” Doctoral dissertation, University of Western Australia.

Zhou, S., Zhou, M., Zhang, X. and Tian, Y. 2021. “Installation of caisson in non-uniform clay interbedded with a sand layer.” Computers and Geotechnics 140:104439. https://doi.org/10.1016/j.compgeo.2021.104439